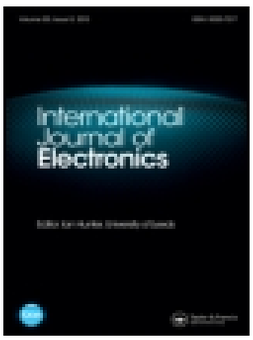

International Journal of Electronics

ISSN: 0020-7217 (Print) 1362-3060 (Online) Journal homepage: http://www.tandfonline.com/loi/tetn20

IDA-PBC control of a DC–AC converter for sinusoidal three-phase voltage generation

Federico M. Serra, Cristian H. De Angelo & Daniel G. Forchetti

To cite this article: Federico M. Serra, Cristian H. De Angelo & Daniel G. Forchetti (2016): IDA-PBC control of a DC–AC converter for sinusoidal three-phase voltage generation, International Journal of Electronics, DOI: 10.1080/00207217.2016.1191087

To link to this article: http://dx.doi.org/10.1080/00207217.2016.1191087

Accepted author version posted online: 21 May 2016.
Published online: 09 Jun 2016.

INTERNATIONAL JOURNAL OF ELECTRONICS, 2016
http://dx.doi.org/10.1080/00207217.2016.1191087

Taylor & Francis
Taylor & Francis Group

IDA-PBC control of a DC–AC converter for sinusoidal three-phase voltage generation

Federico M. Serra[a], Cristian H. De Angelo [b] and Daniel G. Forchetti[b]

[a]Laboratorio de Control Automático (LCA), Universidad Nacional de San Luis - CONICET, Villa Mercedes, San Luis, Argentina; [b]Grupo de Electrónica Aplicada (GEA), Universidad Nacional de Río Cuarto - CONICET, Río Cuarto, Córdoba, Argentina

ABSTRACT

An interconnection and damping assignment (IDA) controller is proposed for regulating the output voltage and frequency of a three-phase DC–AC converter, independently of the supplied load. A modified IDA strategy is used to design the controller, in order to obtain a proper tracking of the reference variables. Moreover, the closed-loop stability is ensured through a proper choice of the desired energy function. Different from classical approaches, such as conventional PI control in *dq* coordinates, the proposed controller provides a better dynamic response while it allows performing a joint design of the voltage and current control loops. Besides, the proposed modified IDA design allows a more precise output voltage control when supplying nonlinear loads, when compared with the classical IDA design. Simulations and experimental results are presented for validating the proposal.

ARTICLE HISTORY
Received 23 July 2014
Accepted 15 May 2016

KEYWORDS
Voltage source converter; DC–AC converter; control design; interconnection and damping assignment; passivity

1. Introduction

The use of DC–AC converters for generating sinusoidal three-phase voltages with low distortion has grown in the last years due to the increasing use of equipment that requires high power quality for proper operation. The most common applications of such converters are uninterruptible power supplies (UPS) used to supply sensitive loads, such as medical equipment, communications or data processing equipment or industrial control equipment, in absence of electrical grid energy (Escobar, Valdez, Leyva-Ramos, & Mattavelli, 2007; Kim & Lee, 2010; Kwona, Choia, & Kwona, 2006; Loh, Newman, Zmood, & Holmes, 2003; Zbigniew Rymarski, 2011; Valderrama, Stankovic, & Mattavelli, 2003); front-end converters for supplying isolated loads from renewable energy generation (Jung et al., 2014; Lee & Jang, 2005; Serra, De Angelo, & Forchetti, 2012a; Singh & Kasal, 2008) and high performance AC power supplies (Li, Jin, & Smedley, 2008; Mattavelli, 2001).

These DC–AC converters generally consist on a three-phase voltage source converter (VSC) and an LC output filter, as shown in Figure 1. The control objective for this converter, although dependent upon the particular application, usually consists in generating a constant amplitude and frequency output voltage, independently of the load condition. In some cases, the adjustment of the output voltage as a function of the load requirement could also be necessary. Then, an adequate control strategy must be designed in order to accomplish these objectives.

In terms of the controller design, it is desirable to use a strategy which allows a flexible design, able to solve the problem of having less control inputs than control variables, while

CONTACT Federico M. Serra serrafederico@gmail.com Laboratorio de Control Automático (LCA), Universidad Nacional de San Luis - CONICET, Villa Mercedes, San Luis, Argentina

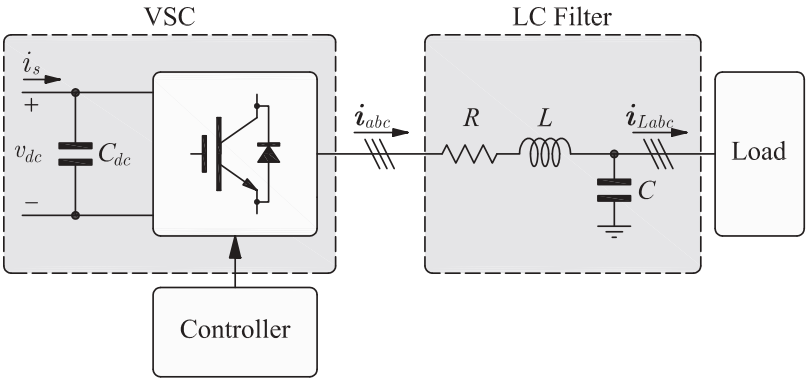

Figure 1. Three-phase DC–AC converter system.

ensuring the system stability. Early proposals used simple proportional integral (PI) controllers, with inner current-control loops and outer voltage-control loops, in order to regulate the output voltage (Haque, Negnevitsky, & Muttaqi, 2010). Even when such controllers are widely known, it is also known that they have problems to cope with load nonlinearities and disturbances. Multi-loop feedback control schemes were also proposed in the literature, by using different measurements in order to improve voltage regulation and disturbance rejection (Loh et al., 2003).

Other strategies propose more complex nonlinear control techniques, like feedback linearisation or dissipativity-based control, in order to obtain a good voltage control performance when supplying nonlinear loads (Kim & Lee, 2010; Valderrama et al., 2003). On the other hand, in many of these proposals, determination of the controller parameters is usually complicated, which implies that in many cases the desired response cannot be achieved in practice.

Passivity-based control (PBC) methods allow the controller design by a systematic procedure, where the system structure is clearly defined. Among these methods, interconnection and damping assignment (IDA) (Ortega, Van Der Schaft, Maschke, & Escobar, 2002) is a strategy which consists on choosing a desired closed-loop energy function in order to ensure that the control error converges to zero. Besides, the determination of controller parameters is simpler than in other strategies.

For these reasons, IDA-based controllers have been proposed for different power converters (Doria-Cerezo, Batlle, & Espinosa-Perez, 2010; Linares-Flores, Reger, & Sira-Ramírez, 2010), including rectifiers (Tang, Yu, & Zou, 2008; Wang, Wang, & Xu, 2008) or inverters (Chen & Ge, 2010; Serra et al., 2012a, 2014). In order to obtain unity power factor, sinusoidal phase currents and constant DC output voltage for a three-phase rectifier, an IDA controller is presented in Wang et al. (2008). Simulation results show that the controller is stable and robust against load variations. For the same system, an integral control loop is added to the IDA controller in Tang et al. (2008), in order to eliminate the steady state error in the DC output. On the other hand, an IDA controller for a grid connected three-phase VSC is designed in Serra et al. (2014), while Chen and Ge (2010) propose a controller for a single-phase inverter, allowing to solve the instability problems introduced by the output filters.

Controlling a three-phase DC–AC converter can be considered a regulation problem when the system is represented in an appropriate rotating reference frame and when the converter supplies a linear load. In such a case, controller references are constant signals and the classical IDA approach can be successfully applied to design a high performance controller (Serra et al. 2012a). However, when the converter supplies a nonlinear load, such design may not be suitable, since for rejecting nonlinear load effects current references must be time-varying signals. For this reason, in this paper the modified IDA approach presented in Wang and Goldsmith (2008) which allows dealing with tracking problems, is used to design the controller.

Thus, the design of a control strategy for a three-phase DC–AC converter is performed using modified IDA, with the aim of regulating the amplitude and frequency of the output voltage, independently of the converter load. The proposed energy-based design is a systematic design method that, unlike other strategies, can give physical interpretation to the control action. In addition, this method provides a better visualisation of the system structure allowing an intuitive cancellation of unwanted couplings between the dynamics of the system, while assigning the damping required to achieve the desired convergence rate.

The performance of the proposed control strategy is compared with conventional PI controllers in *dq* coordinates and it is validated by simulation and experimental results performed on an experimental VSC prototype. Results demonstrate that the proposed controller provides a better dynamic response and it is more robust to certain disturbances. It also allows performing a joint design of the voltage and current control loops, while providing limits for the gains of each loop. Additionally, the proposed controller is compared with the classical IDA design (Serra et al. 2012a), in order to demonstrate the improved performance when the converter supplies a nonlinear load.

The paper is organised as follows. Section 2 introduces the converter model in *dq* coordinates and its port-Hamiltonian representation. The proposed control strategy based on IDA is developed in Section 3. Section 4 shows simulation results obtained under different loads and operating conditions, while Section 5 presents experimental results obtained from the laboratory prototype. Finally, the obtained results are discussed in Section 6, and conclusions are drawn in Section 7.

2. System configuration and model

The considered DC–AC converter is shown in Figure 2. It is composed by a VSC, comprising the six IGBTs ($S_1 \ldots S_6$), and an LC output filter. Here, the equivalent resistance R represents the losses of the filter inductance and the VSC.

The input DC-link voltage, v_{dc}, is considered approximately constant, or at least slowly variant depending on the input power. This assumption is valid since in the considered applications (mentioned in section 1) DC-link voltage can be produced by either a battery or a renewable source (e.g. fuel-cell, wind turbine, solar panel), which usually employs a power electronic converter in the source side, in order to adjust the output voltage.

The DC–AC converter model in *dq* coordinates is the following,

$$L\dot{i}_d = m_d v_{dc} - Ri_d - \omega_{dq} L i_q - e_d, \tag{1}$$

$$L\dot{i}_q = m_q v_{dc} - Ri_q + \omega_{dq} L i_d - e_q, \tag{2}$$

$$C\dot{e}_d = i_d - \omega_{dq} C e_q - i_{Ld}, \tag{3}$$

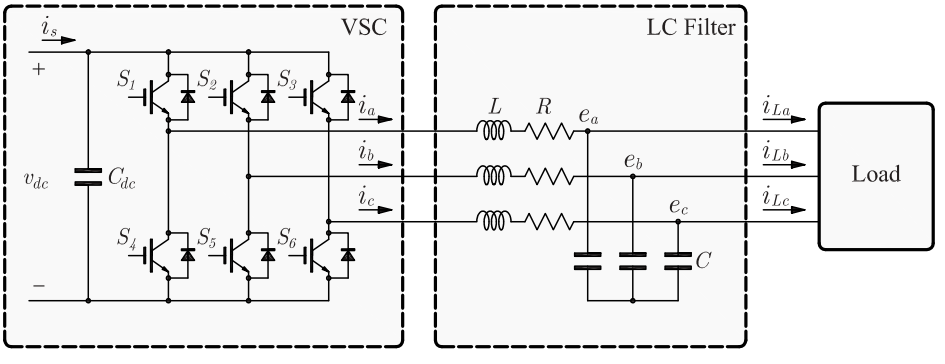

Figure 2. Three-phase DC–AC converter.

$$C\dot{e}_q = i_q + \omega_{dq} C e_d - i_{Lq}. \tag{4}$$

Here, ω_{dq} is the angular frequency of the dq reference frame that is set equal to the desired output-voltage frequency. i_d and i_q represent the currents in the dq frame; e_d and e_q are the output voltages; i_{Ld} and i_{Lq} correspond to the load currents; while m_d and m_q are the inverter modulation indexes. All the variables represented in the dq reference frame are obtained through Park's transformation from the abc variables. Parameters L, C and R represent inductance, capacitance of the output filter, and the equivalent output resistance which models the filter inductance losses and the converter losses.

For designing the VSC controller using the IDA approach, the complete system is represented by its port-Hamiltonian (pH) model (Ortega et al., 2002).

$$\dot{\mathbf{x}} = [\mathbf{J}(\mathbf{x}) - \mathbf{R}(\mathbf{x})] \frac{\partial H(\mathbf{x})}{\partial \mathbf{x}} + \mathbf{g}(\mathbf{x})\mathbf{u} + \boldsymbol{\zeta}, \tag{5}$$

where the state vector is $\mathbf{x}$, $\mathbf{J}(\mathbf{x})$ and $\mathbf{R}(\mathbf{x})$ are the interconnection and damping matrices, respectively, $H(\mathbf{x})$ represents the total energy stored in the system, $\mathbf{g}(\mathbf{x})$ is the input matrix, $\mathbf{u}$ is the control input vector, and $\boldsymbol{\zeta}$ represents the system disturbances.

The pH model of the DC–AC converter is,

$$\begin{bmatrix} L\dot{i}_d \\ L\dot{i}_q \\ C\dot{e}_d \\ C\dot{e}_q \end{bmatrix} = \begin{bmatrix} -R & -\omega_{dq}L & -1 & 0 \\ \omega_{dq}L & -R & 0 & -1 \\ 1 & 0 & 0 & -\omega_{dq}C \\ 0 & 1 & \omega_{dq}C & 0 \end{bmatrix} \begin{bmatrix} i_d \\ i_q \\ e_d \\ e_q \end{bmatrix} + \begin{bmatrix} v_{dc} & 0 \\ 0 & v_{dc} \\ 0 & 0 \\ 0 & 0 \end{bmatrix} \begin{bmatrix} m_d \\ m_q \end{bmatrix} + \begin{bmatrix} 0 \\ 0 \\ -i_{Ld} \\ -i_{Lq} \end{bmatrix}. \tag{6}$$

In this case, interconnection and damping matrices $\mathbf{J}$ and $\mathbf{R}$ do not depend on the states,

$$\mathbf{J} = \begin{bmatrix} 0 & -\omega_{dq}L & -1 & 0 \\ \omega_{dq}L & 0 & 0 & -1 \\ 1 & 0 & 0 & -\omega_{dq}C \\ 0 & 1 & \omega_{dq}C & 0 \end{bmatrix}, \tag{7}$$

$$\mathbf{R} = \begin{bmatrix} R & 0 & 0 & 0 \\ 0 & R & 0 & 0 \\ 0 & 0 & 0 & 0 \\ 0 & 0 & 0 & 0 \end{bmatrix}, \tag{8}$$

where $\mathbf{J} = -\mathbf{J}^T$ is antisymmetric and $\mathbf{R} = \mathbf{R}^T \geq 0$ is symmetric positive semidefinite. The total energy stored in the system, H ($\mathbf{x}$), is given by the sum of the energy stored on the output filter inductors and capacitors,

$$H(\mathbf{x}) = \frac{1}{2}\left(Li_d^2 + Li_q^2 + Ce_d^2 + Ce_q^2\right). \tag{9}$$

3. Controller design

In several applications of VSC, the control objective consists in regulation to a constant set point (e.g. a rectifier with constant DC output voltage or an inverter with constant output voltage represented in a synchronous reference frame). In such cases, the controller can be designed using the classic IDA approach proposed in Ortega et al. (2002). However, if sudden changes in the output voltage are required, or for a better rejection to load changes or nonlinear loads effects, the controller design can be posed as a trajectory tracking problem, with variable references which depend on load and set points.

Then, instead of considering a fixed equilibrium point, the controller is designed so as to make the system state variables follow the trajectory defined by a reference vector,

$$\mathbf{x}^* = \begin{bmatrix} Li_d^* & Li_q^* & Ce_d^* & Ce_q^* \end{bmatrix}^T, \tag{10}$$

while ensuring that the tracking error ($\boldsymbol{\epsilon} = \mathbf{x} - \mathbf{x}^*$) converges to zero.

This objective can be achieved by setting the closed-loop dynamic of the tracking error as follows,

$$\dot{\boldsymbol{\epsilon}} = [\mathbf{J}_d(\boldsymbol{\epsilon}) - \mathbf{R}_d(\boldsymbol{\epsilon})] \frac{\partial H_d(\mathbf{x}, \mathbf{x}^*)}{\partial \boldsymbol{\epsilon}}, \tag{11}$$

with $\mathbf{J}_d(\boldsymbol{\epsilon}) = \mathbf{J}(\boldsymbol{\epsilon}) + \mathbf{J}_a(\boldsymbol{\epsilon})$ and $\mathbf{R}_d(\boldsymbol{\epsilon}) = \mathbf{R}(\boldsymbol{\epsilon}) + \mathbf{R}_a(\boldsymbol{\epsilon})$, being $\mathbf{J}_a(\boldsymbol{\epsilon})$ and $\mathbf{R}_a(\boldsymbol{\epsilon})$ the matrices used to design the control strategy.

$H_d(\mathbf{x}, \mathbf{x}^*)$ is the new energy function (Hamiltonian) for the closed-loop system which has a stable equilibrium at $\boldsymbol{\epsilon} = 0$ (Wang & Goldsmith, 2008). This equilibrium will be asymptotically stable if $H_d(\mathbf{x}, \mathbf{x}^*)$ has a minimum in **x***, that is,

$$\left.\frac{\partial H_d(\mathbf{x}, \mathbf{x}^*)}{\partial \mathbf{x}}\right|_{\mathbf{x}=\mathbf{x}^*} = 0, \left.\frac{\partial^2 H_d(\mathbf{x}, \mathbf{x}^*)}{\partial \mathbf{x}^2}\right|_{\mathbf{x}=\mathbf{x}^*} > 0. \tag{12}$$

The closed-loop energy function (13) is chosen so as to ensure the closed-loop stability and the convergence of the tracking error,

$$H_d(\mathbf{x}, \mathbf{x}^*) = \frac{1}{2}(\boldsymbol{\epsilon}^T \mathbf{P}^{-1} \boldsymbol{\epsilon}). \tag{13}$$

The time derivative of $H_d(\mathbf{x}, \mathbf{x}^*)$ is given by,

$$\dot{H}_d(\mathbf{x}, \mathbf{x}^*) = -\boldsymbol{\epsilon}^T \mathbf{P}^{-1} \mathbf{R}_d \mathbf{P}^{-1} \boldsymbol{\epsilon} < 0, \tag{14}$$

with,

$$\mathbf{P} = \begin{bmatrix} L & 0 & 0 & 0 \\ 0 & L & 0 & 0 \\ 0 & 0 & C & 0 \\ 0 & 0 & 0 & C \end{bmatrix}. \tag{15}$$

From (14) it can be seen that convergence to zero of the tracking error can be ensured if $\mathbf{R}_d$ is a positive definite matrix. For this reason, $\mathbf{R}_a$ is chosen as follows,

$$\mathbf{R}_a = \mathbf{R}_a^T = \begin{bmatrix} R_1 & 0 & 0 & 0 \\ 0 & R_2 & 0 & 0 \\ 0 & 0 & R_3 & 0 \\ 0 & 0 & 0 & R_4 \end{bmatrix}, \tag{16}$$

while R_1, R_2, R_3, R_4, are selected in order to obtain the desired convergence speed.

Furthermore, $\mathbf{J}_a$ is designed so as to decouple voltage and current equations on d and q axes, that is,

$$\mathbf{J}_a = \begin{bmatrix} 0 & \omega_{dq} L & 0 & 0 \\ -\omega_{dq} L & 0 & 0 & 0 \\ 0 & 0 & 0 & \omega_{dq} C \\ 0 & 0 & -\omega_{dq} C & 0 \end{bmatrix}. \tag{17}$$

Even when there are other possible choices of $\mathbf{J}_a$, the one proposed in this work results in decoupled error dynamics, which simplifies the determination of controller gains and has advantages regarding closed-loop performance.

Using (5) and (11), and taking into account that,

$$H_a(\mathbf{x}, \mathbf{x}^*) = H_d(\mathbf{x}, \mathbf{x}^*) - H(\mathbf{x}), \tag{18}$$

the differential equation below is obtained,

$$[\mathbf{J} - \mathbf{R}] \frac{\partial H_a(\mathbf{x}, \mathbf{x}^*)}{\partial \boldsymbol{\epsilon}} + [\mathbf{J}_a - \mathbf{R}_a] \frac{\partial H_d(\mathbf{x}, \mathbf{x}^*)}{\partial \boldsymbol{\epsilon}} - \boldsymbol{\zeta} + \mathbf{x}^* = \mathbf{g}(\mathbf{x})\mathbf{u}. \tag{19}$$

By solving (19), the expressions for modulation indices m_d and m_q results in,

$$m_d = \frac{L\dot{i}_d^* + Ri_d^* + \omega_{dq} L i_q - R_1(i_d - i_d^*) + e_d^*}{v_{dc}}, \tag{20}$$

$$m_q = \frac{L\dot{i}_q^* + Ri_q^* - \omega_{dq} L i_d - R_2(i_q - i_q^*) + e_q^*}{v_{dc}}, \tag{21}$$

while references for the dq currents are,

$$i_d^* = C\dot{e}_d^* - R_3(e_d - e_d^*) + \omega_{dq} C e_q + i_{Ld}, \tag{22}$$

$$i_q^* = C\dot{e}_q^* - R_4(e_q - e_q^*) - \omega_{dq} C e_d + i_{Lq}. \tag{23}$$

Since (20)–(23) include derivatives of the reference trajectories, a better tracking of the references is obtained. This allows both, a better tracking of reference voltage changes, and an improved performance under load disturbances and nonlinear load effects, when compared with other control strategies such as the classical IDA approach (Serra et al., 2012a). These derivatives are calculated using high-gain observers (Dabroom & Khalil, 1997) in the controller implementation.

It must be noted that the obtained control law is similar to a PD controller with some feedforward terms. However, in contrast with conventional PD controllers, the proposed controller includes derivatives of the reference trajectories and some measured signals, but not all of them. This makes it advantageous in terms of the implementation of derivatives of noisy signals, when compared with conventional PD controllers. Besides, there are some advantages regarding the design method, which allows ensuring closed-loop stability and an easier methodology for controller gain design.

With (20)–(23), the error dynamics are given by,

$$\dot{\epsilon}_{i_d} = -\frac{(R + R_1)}{L}\epsilon_{i_d} - \frac{1}{C}\epsilon_{e_d}, \tag{24}$$

$$\dot{\epsilon}_{i_q} = -\frac{(R + R_2)}{L}\epsilon_{i_q} - \frac{1}{C}\epsilon_{e_q}, \tag{25}$$

$$\dot{\epsilon}_{e_d} = \frac{1}{L}\epsilon_{i_d} - \frac{R_3}{C}\epsilon_{e_d}, \tag{26}$$

$$\dot{\epsilon}_{e_q} = \frac{1}{L}\epsilon_{i_q} - \frac{R_4}{C}\epsilon_{e_q}. \tag{27}$$

As can be seen, error dynamics on d axis, given by (24) and (26), are independent from error dynamics on q axis ((25) and (27)). Then, from (24) and (26), a second order differential equation for the d axis voltage error can be obtained. By specifying the desired settling time and damping ratio, gains R_1 and R_3 can be calculated equating the obtained second order system with the desired one. The same procedure is used to obtain R_2 and R_4.

The reference vector $\mathbf{x}^*$ is designed in order to meet the control objectives. Therefore, e_d^* is set constant while e_q^* is set to 0, so as to control the output voltage amplitude. Besides, ω_{dq} is selected equal to the desired output frequency.

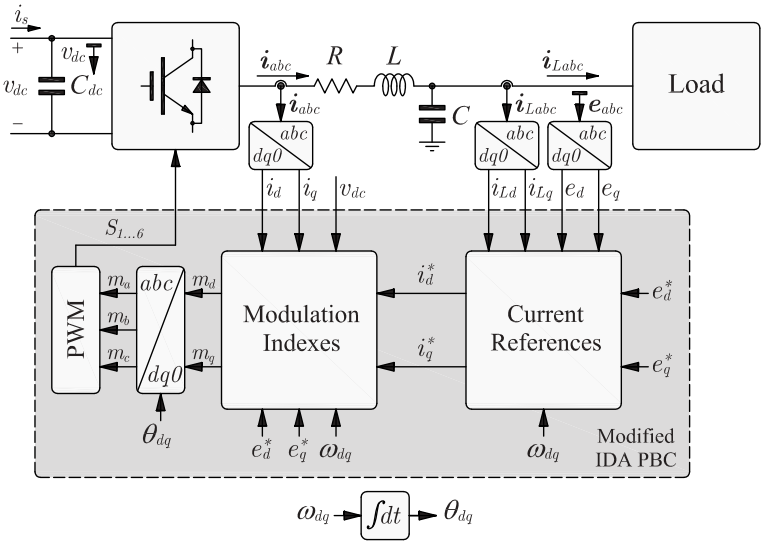

Figure 3. Proposed control strategy.

It must be noted that the assumption of constant DC voltage, v_{dc}, simplifies the system model into a linear one. This makes it easier to solve the matching equation at the controller design stage without affecting the overall system behaviour. Even if the DC voltage presents some ripple or other disturbances, they could introduce a greater output current ripple, but the controller performance will not be affected. In the case of changes in the mean value of the DC voltage, since this value is measured, such changes will not affect the controller performance, provided that the DC value is enough to produce the output voltage in the inverter. However, if one wants to consider a variable DC voltage, the control input can be expressed as the product of the DC voltage (measured) and the modulation indexes, resulting in the same linear problem. Otherwise, the system can be extended in order to consider the DC-link dynamics, by choosing v_{dc} as a state variable, which results in a nonlinear system that can also be solved using the IDA-PBC approach (as in Serra et al. (2014); Tang et al. (2008)).

The proposed control strategy is summarised in Figure 3.

4. Simulation results

The proposed controller was validated through simulation results obtained in SimPowerSystems of Matlab™. The simulated converter includes switching effect, losses and a detailed transistor model. For comparing the proposed IDA controller with existing control methods, results obtained with a conventional Proportional + Integral (PI) controller in *dq* coordinates are also presented.

The control objective is to ensure that the output voltage has constant amplitude and frequency. Consequently, the VSC was subjected to load changes and connection of different types of load, so as to evaluate its performance under such conditions. Even though there are applications where it is necessary to adjust the amplitude of the output voltage depending on the load requirements. Such situation was also considered both in simulation and experiments.

Parameters of the controllers (IDA and conventional PI controller) used to obtain the simulation results are shown in Table 1, while the converter specifications are detailed in Table 2.

In the first test, a resistive load ($R_L = 47\Omega$) was connected to the VSC. At $t = 50$ms, the load resistance is reduced to $R_L = 23.5\Omega$. Figure 4(a) shows the *d* axis output voltage, e_d, (solid line) and its reference (dashed line); Figure 4(b) shows e_q voltage (solid line) and its reference (dashed line). i_d

Table 1. Controller parameters.

Parameter	Value
R_1, R_2	5.99
R_3, R_4	0.132
K_{pi}	40,000
K_{ii}	100
K_{pv}	0.05
K_{iv}	30

Table 2. DC–AC converter specifications.

Parameter	Value
DC-link voltage (v_{dc})	430 V
Filter inductance (L)	4 mH
Filter resistance (R)	0.2 Ω
Filter capacitance (C)	45 μF
DC-link capacitance (C_{dc})	4700 μF
Internal IGBT resistance ($R_{on(IGBT)}$)	2.6 mΩ
Switching frequency (f_s)	10 kHz
Output frequency (f)	50 Hz
Rated power (P)	2 kVA

and i_q currents with their references are shown in Figure 4(c). In Figure 4(d), phase a output voltage and the corresponding load current are shown.

As shown in Figure 4(a,b), voltages on the output capacitor (e_d and e_q) remain in their reference value up to the moment in which the load changes. At this time, e_d and e_q present a short transient (about 2.5 ms), until the controller sets the new value for the output current reference, as seen in Figure 4(c).

Figure 4(d) shows capacitor voltage and load current of phase a, where an increase in the current amplitude at t = 50 ms due to the load change is appreciated. As it can be observed, voltage and current waveforms are sinusoidal without significant distortions.

The response of the proposed IDA controller (black line) is compared with a conventional PI controller in dq coordinates (green line) in Figure 5 for the same test. The voltage-loop PI controllers were adjusted to obtain a settling time similar to the IDA controller, while current-loop PI controllers are about 10 times faster. Higher PI gains are not practical and produce an undesired response. It must be noted that the proposed controller provides a faster response time against load changes. Moreover, both currents and voltages on the d and q axis are decoupled using the proposed controller.

Figure 6 shows the same case as Figure 4 but considering a mismatch between the model and controller parameters. A 25% decrease on the filter inductance, a 25% increase on the filter resistance and a 10% increase on the filter capacitance are considered for this test.

As can be appreciated in Figure 6(a,b), d and q axis voltages present small steady state errors due to the introduced parameter mismatch. However, it must be noted that the dynamic closed-loop response is not affected. Figure 6(c) shows that the error introduced in the d and q currents is negligible in this case.

In case of greater parameter variations, or when the steady state error is not acceptable, controller robustness can be improved by adding an integral action controller using the same IDA design technique, as presented in Serra et al. (2014).

The second test consists in a change in the reference of the output voltage amplitude. The system is working in steady state and at t = 50 ms, the d axis reference voltage is reduced to 62.5%. Figure 7(a) shows the e_d output voltage (solid line) with its reference (dashed line); Figure 7(b) shows the e_q output voltage (solid line) with its reference (dashed line); Figure 7(c) presents currents i_d and i_q with their references; and Figure 7(d) shows the output voltage and load current at phase a.

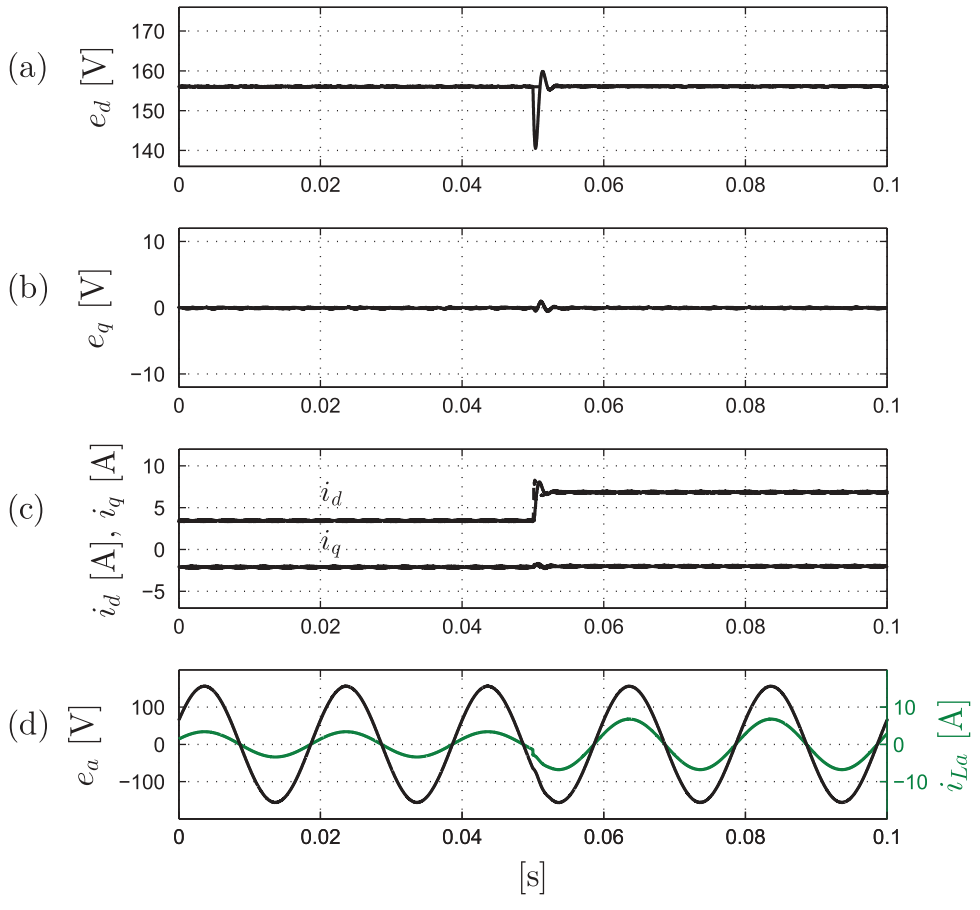

Figure 4. Resistive load change. (a) voltage e_d, (b) voltage e_q, (c) currents i_d and i_q, (d) voltage e_a (black) and current i_{La} (green).

As shown in Figure 7(a,b), voltages on the output capacitor remain in their reference value up to the moment in which the reference e_d^* changes. At this time, a brief transient appears on e_d and e_q voltages, up to the moment when the controller sets the new currents due to the output voltage change.

Figure 7(d) shows a reduction in the phase *a* voltage amplitude at t = 50 ms due to the reference change. As can be observed, voltage and current waveforms are sinusoidal without significant distortions.

A third simulation test is performed in order to check the behaviour of the proposed controller when the converter is supplying a nonlinear load. Such load is composed by a three-phase rectifier feeding a resistive load R_L = 116.5 Ω. Figure 8 shows the output voltage and load current at phase *a*. As shown, amplitude and frequency of the output voltage are controlled within the reference values, while the distortion in the voltage waveform remains between admissible limits.

5. Experimental results

Experimental tests were performed in order to validate the proposed control strategy. The 2 kVA experimental prototype consists of a three-phase inverter composed by 1200 V–75 A IGBTs (SKM75GB124D), and the control strategy was implemented on a Texas Instrument TMS320F28335 DSP. Filter parameters are the same used for obtaining the simulation results

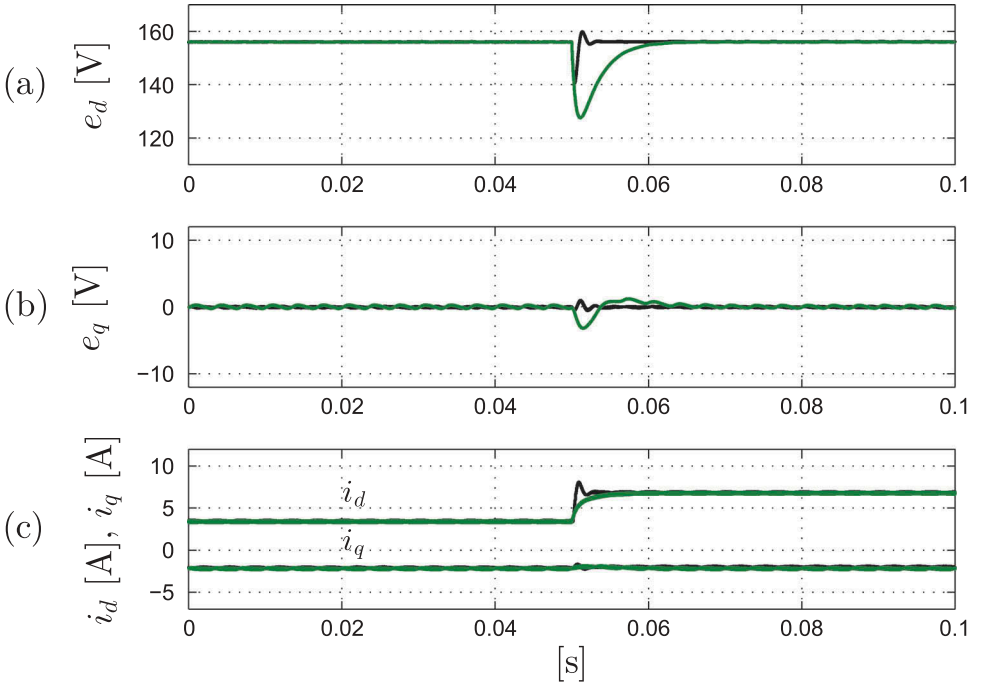

Figure 5. Resistive load change with the proposed controller (black line) and a conventional PI controller (green line). (a) voltage e_d, (b) voltage e_q, (c) currents i_d and i_q.

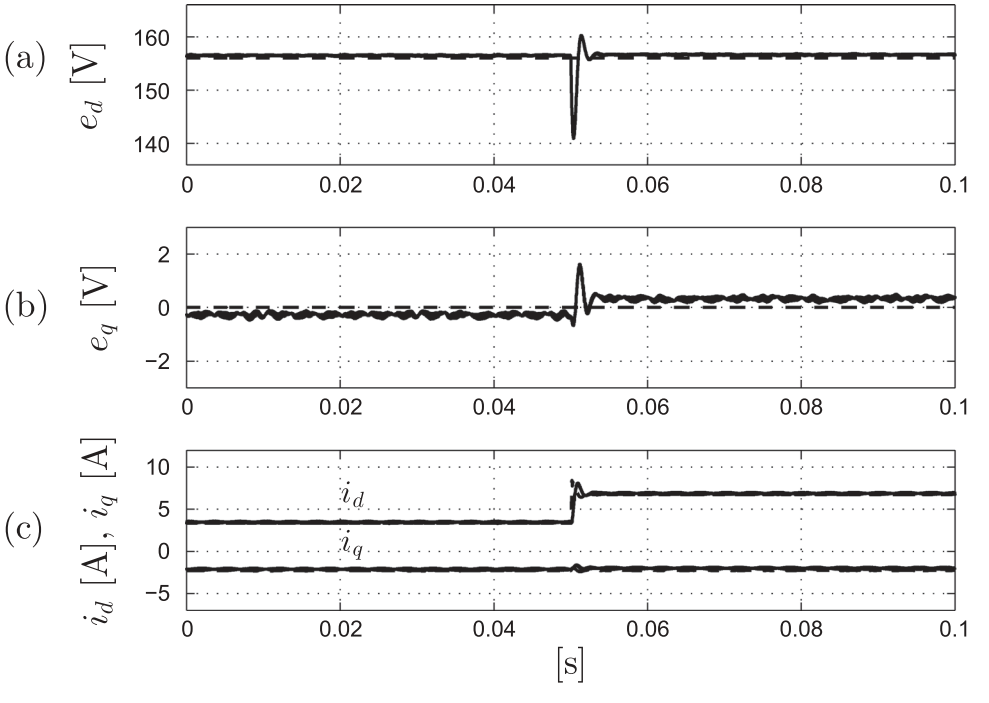

Figure 6. Resistive load change with parameter mismatch. (a) voltage e_d, (b) voltage e_q, (c) currents i_d and i_q.

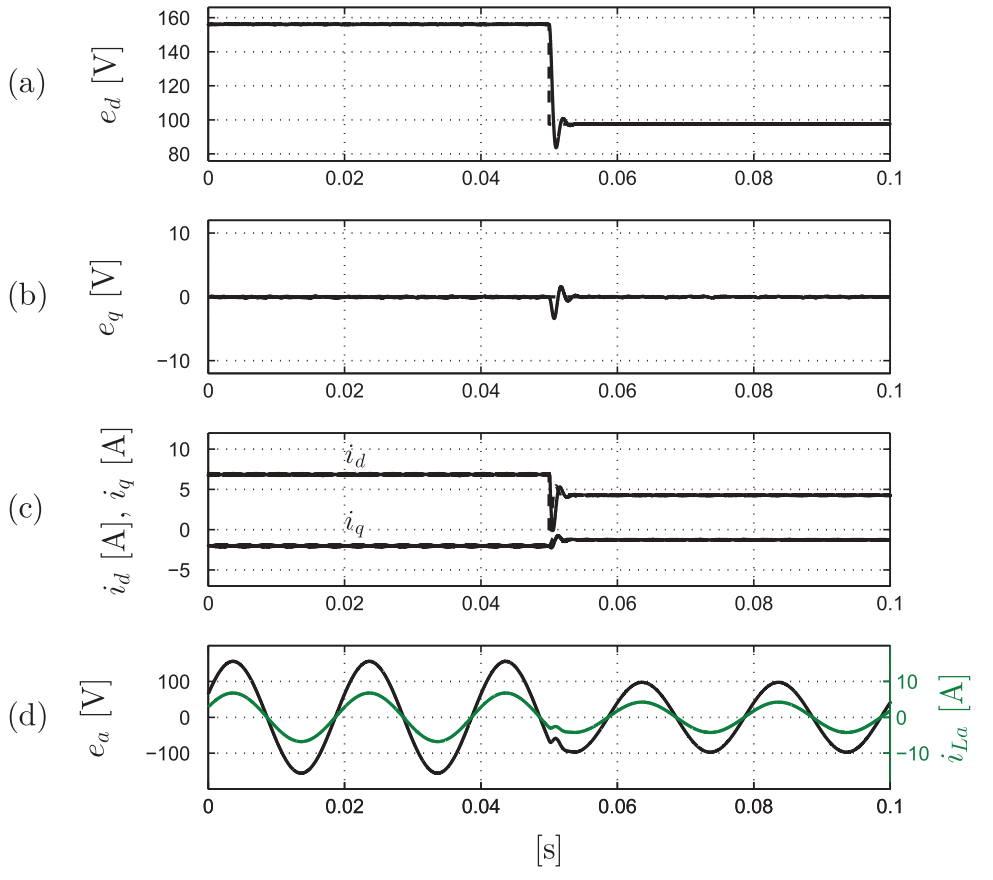

Figure 7. Output voltage reference change. (a) voltage e_d, (b) voltage e_q, (c) currents i_d and i_q, (d) voltage e_a (black) and current i_{La} (green).

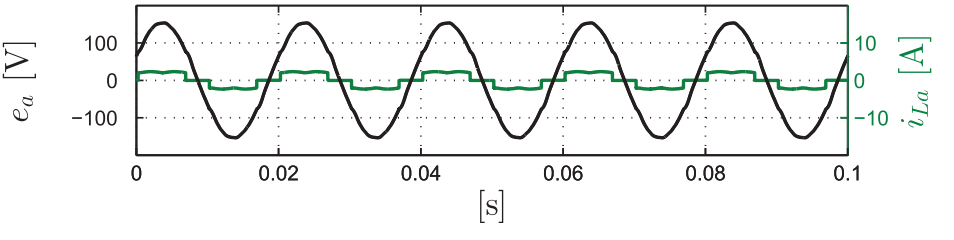

Figure 8. Nonlinear load test. Voltage e_a (black) and current i_{La} (green).

(Table 2). A sinusoidal PWM with 10 kHz switching frequency, with a 430 V DC-link was used in the implemented prototype.

Three-phase output voltage of the DC–AC converter supplying a 23.5 Ω resistive load is shown in Figure 9. It can be seen that this voltage has constant amplitude (110 Vrms) and frequency (50 Hz), as desired.

Figure 10 shows the frequency spectrum of the output voltage. In this spectrum, negative frequency means negative sequence component. As can be seen, harmonic components are very low with an amplitude lower than 2%. The output voltage THD is 1.86%, which is lower than the values established by IEC 62040-3 (less than 8%) [IEC 62040-3 (1999)].

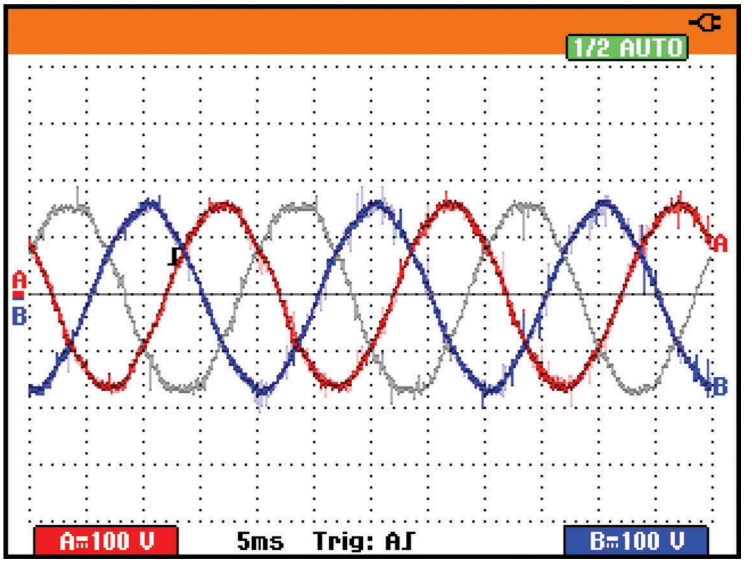

Figure 9. Three-phase output voltage $e_{abc.}$

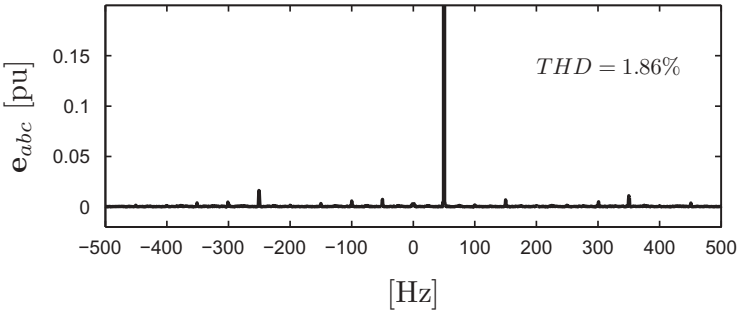

Figure 10. Frequency spectrum of output voltage $e_{abc.}$

With the aim of validating the simulation results presented in Section 4, experimental tests were performed reproducing the same situations.

Figure 11 shows the output capacitor voltage and the load current for phase *a* corresponding to a resistive load change, from R_L = 47 Ω to R_L = 23.5 Ω at t = 30 ms. As shown in this figure, the amplitude of the load current grows due to the load change. Besides, it is important to remark that the amplitude and frequency of the output voltage remain constant even when the load changes. In this case, the output voltage THD measured in steady state before the load change is 1.55%, while the one measured after load change is the same as in Figure 10.

Figure 12 shows the results obtained for the same test (resistive load change) but using conventional PI controllers in *dq* coordinates. Even when the conventional controller allows maintaining constant output voltage and frequency, voltage transient after load change is longer, as was shown in Figure 5. Moreover, output voltage waveform is more distorted than for the modified IDA controller (THD = 2.15%, before load change). This is due to the fact that proposed IDA-based design allows decoupling *d* and *q* axis, while the conventional controller does not ensure such decoupling. A deeper discussion about differences between the proposed controller and previous proposals is presented in the next section.

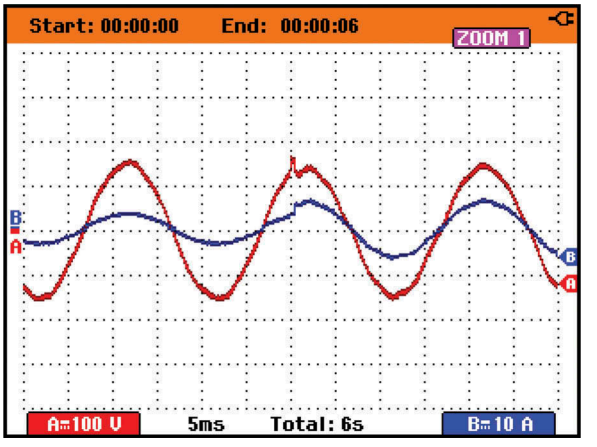

Figure 11. Resistive load change using the proposed IDA controller. Voltage e_a (Channel A) and current i_{La} (Channel B).

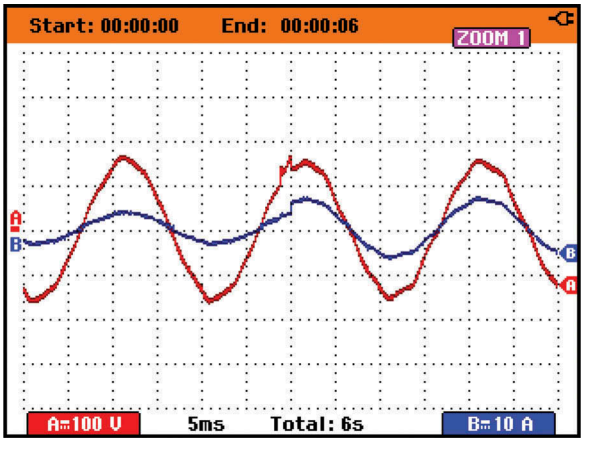

Figure 12. Resistive load change using conventional *dq* PI controllers. Voltage e_a (Channel A) and current i_{La} (Channel B).

The test in which the output voltage reference is reduced to 62.5% at t = 30 ms is shown in Figure 13. This test allows demonstrating that the proposed control strategy is able to adjust the output voltage amplitude when the application requires this feature. As can be seen, the output voltage amplitude follows its reference, while its frequency is maintained constant. In this case, the voltage THD measured after the amplitude reduction in steady state is 1.57 %.

In order to test the performance of the proposed control strategy when the converter supplies an inductive load, Figure 14 shows output voltage and current when the load consists of an induction motor. At t = 30 ms, the voltage reference is reduced, thus showing the transient response of the controller. As it can be observed, the proposed modified IDA strategy allows controlling amplitude and frequency of the motor voltage. In this case, output voltage THD is 0.72%.

Figure 15 corresponds to the test in which a nonlinear load is connected to the converter. Even when the nonlinear load affects the output voltage waveform, voltage distortion is very small. The frequency spectrum of the output voltage is shown in Figure 16. In this case, voltage THD is below 4%, which is a value accepted by standards.

For comparison purposes, Figure 17 shows converter output voltage and current when supplying the same nonlinear load, but using the classical IDA controller as proposed in Serra et al.

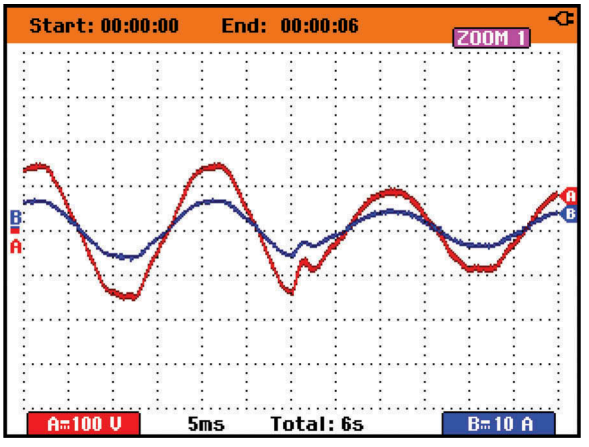

Figure 13. Voltage reference change, resistive load. Voltage e_a (Channel A) and current i_{La} (Channel B).

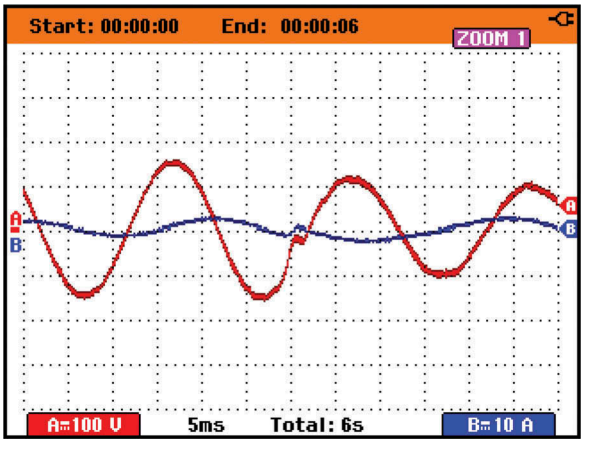

Figure 14. Voltage reference change, inductive load. Voltage e_a (Channel A) and current i_{La} (Channel B).

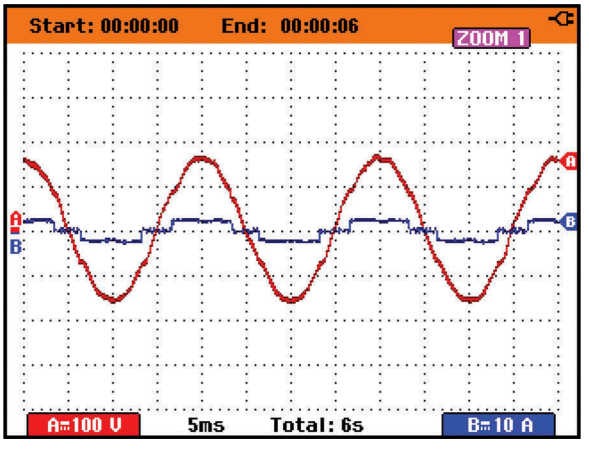

Figure 15. Nonlinear load using the proposed IDA controller. Voltage e_a (Channel A) and current i_{La} (Channel B).

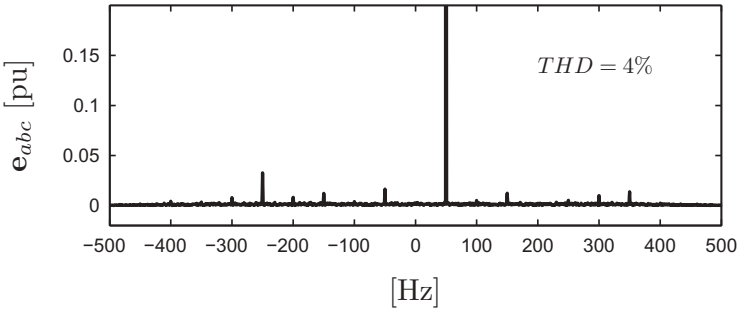

Figure 16. Nonlinear load using the proposed IDA controller. Frequency spectrum of output voltage e_{abc}.

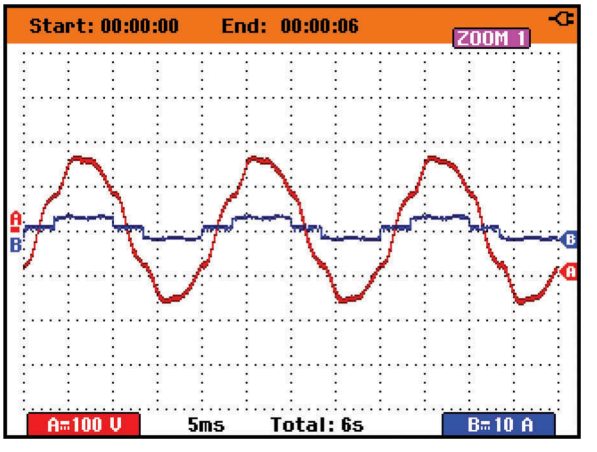

Figure 17. Nonlinear load using the classical IDA approach. Voltage e_a (Channel A) and current i_{La} (Channel B).

(2012a). In this case, voltage waveform shows a greater distortion than the one in Figure 15. Frequency spectrum for this case is shown in Figure 18, where the THD is 7.2%, close to the maximum value allowed by standards.

These last tests show that the controller proposed in this paper, using the modified IDA approach, allows a better performance when the converter supplies nonlinear loads, even when compared with other nonlinear control strategies.

6. Discussion

The energy-based design methodology proposed in this paper has numerous advantages not only from the point of view of design procedure but also concerning performance of the controller.

Regarding design procedure, IDA is a systematic methodology that provides physical interpretation to the control action, which in turn allows establishing the stability conditions of the system and facilitates the determination of the controller parameters. The controller design, following the steps of the IDA strategy, is an organised design by matrix equations, where each matrix has a well-defined physical meaning. In this way, the designer can modify the structure of the system to simplify the problem of having a greater number of control variables than control actions.

Concerning control performance, when the modified IDA controller is compared to well-known strategies such as conventional PI control in *dq* coordinates, it is observed that IDA provides a better dynamic response and is more robust to certain disturbances (such as converter dead time) (see Figures 5 and 12). This is due to the fact that this strategy allows decoupling of the *d* and *q*

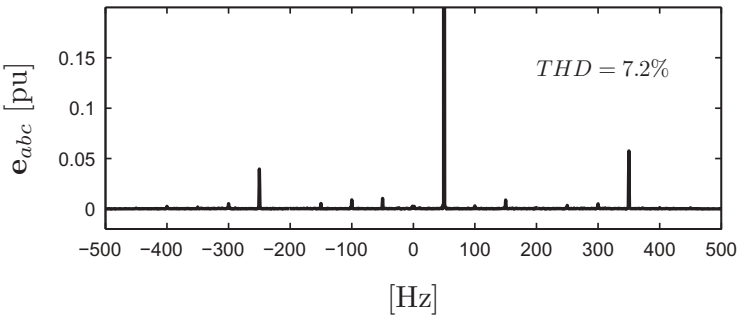

Figure 18. Nonlinear load using the classical IDA approach. Frequency spectrum of output voltage e_{abc}.

axes. It also allows performing a joint design of the voltage and current control loops, while providing limits for the gains of each loop. On the other hand, in the conventional control in *dq* coordinates, the determination of the controller parameters is more complicated, which implies that in many cases the desired response times cannot be achieved.

Besides the conventional PI controller in *dq* coordinates, the proposed controller was compared with a more complex strategy (controller design using the classical IDA approach). As it was observed in the experimental tests, the proposed controller using the modified IDA design allows obtaining a better performance when the converter supplies a nonlinear load.

If the proposed controller is compared with other strategies like feedback linearisation, it can be observed that besides obtaining a better rejection to nonlinear load effects, the proposed design using IDA has also advantages regarding design procedure, as mentioned in Serra, De Angelo, Forchetti and Garcia (2012b). When compared with other techniques for controller design, like those based in multiple reference frames (Mattavelli, 2001) or the controller proposed in Mattavelli, Escobar, and Stankovic (2001), even when they provide a good rejection to load harmonics, their implementation and controller adjustments result more complicated than the one proposed in this paper. A more recent proposal (Escobar et al., 2007) allows a simpler implementation, which can be comparable with the present proposal. A newest adaptive technique was recently proposed in Jung et al. (2014), which is robust to system uncertainties, but controller parameters calculation is harder.

7. Conclusions

A new controller for a three-phase DC–AC converter has been proposed using the modified IDA technique.

For the proposed controller, simulation and experimental results were performed in order to validate the proposal. The proposed controller was tested under resistive load changes, voltage reference changes, and for the case of supplying an inductive and a nonlinear load. The obtained results demonstrate that the proposed controller allows a precise control of the output voltage amplitude and frequency, even under changes in the converter load.

Besides, the waveform of the output voltage obtained with the proposed controller results practically sinusoidal, without significant distortions, even when supplying nonlinear loads.

Following the proposed design, a proper choice of the desired energy function allows ensuring the closed-loop system stability. This is realised with an adequate design of the desired interconnection and damping matrices.

Disclosure statement

No potential conflict of interest was reported by the authors.

Funding

This work was supported by the Universidad Nacional de San Luis; Universidad Nacional de Río Cuarto; FONCyT-ANPCyT; and the Consejo Nacional de Investigaciones Científicas y Técnicas (CONICET).

ORCID

Cristian H. De Angelo http://orcid.org/0000-0001-8080-927X

References

Chen, Z.-X., & Ge, L.-S. (2010). Research on current control strategy for grid-connected inverter based on passivity based control. In *Proceedings of the IEEE Energy Conversion Congress and Exposition (ECCE)* (pp. 79–83). Atlanta, GA: IEEE.

Dabroom, A., & Khalil, H. K. (1997). Numerical differentiation using high-gain observers. In *Proceedings of the IEEE 36th Conf. on Decision and Control (CDC)* (pp. 4790–4795). San Diego, CA: IEEE.

Doria-Cerezo, A., Batlle, C., & Espinosa-Perez, G. (2010). Passivity-based control of a wound-rotor synchronous motor. *IET Control Theory and Applications*, *4*(10), 2049–2057. doi:10.1049/iet-cta.2009.0641

Escobar, G., Valdez, A. A., Leyva-Ramos, J., & Mattavelli, P. (2007). Repetitive-based controller for a UPS inverter to compensate unbalance and harmonic distortion. *IEEE Transactions on Industrial Electronics*, *54*(1), 504–510. doi:10.1109/TIE.2006.888803

Haque, M. E., Negnevitsky, M., & Muttaqi, K. M. (2010). A novel control strategy for a variable-speed wind turbine with a permanent-magnet synchronous generator. *IEEE Transactions on Industry Applications*, *46*(1), 331–339. doi:10.1109/TIA.2009.2036550

IEC 62040-3. 1999. Uninterruptible Power Systems (UPS) – part 3: Method of specifying the performance and test requirements. In *International standard IEC 62040-3*. 1st ed. Geneva: IEC.

Jung, J.-W., Vu, N.-T.-T., Dang, D. Q., Do, T. D., Choi, Y.-S., & Choi, H. H. (2014). A three-phase inverter for a standalone distributed generation system: Adaptive voltage control design and stability analysis. *IEEE Transactions on Energy Conversion*, *29*(1), 46–56. doi:10.1109/TEC.2013.2288774

Kim, D.-E., & Lee, D.-C. (2010). Feedback linearization control of three-phase UPS inverter systems. *IEEE Transactions on Industrial Electronics*, *57*(3), 963–968. doi:10.1109/TIE.2009.2038404

Kwona, J.-M., Choia, J.-H., & Kwona, B.-H. (2006). High performance series-parallel type on-line UPS. *International Journal of Electronics*, *93*(4), 207–222. doi:10.1080/00207210600560417

Lee, D.-C., & Jang, J.-I. (2005). Output voltage control of PWM inverters for stand-alone wind power generation systems using feedback linearization. In *Proceedings of the industry applications conference, IAS annual meeting* (Vol. *3*, pp. 1626–1631). Hong Kong: IEEE.

Li, L., Jin, T., & Smedley, K. M. (2008). A new analog controller for three-phase voltage generation inverter. *IEEE Transactions on Industrial Electronics*, *55*(8), 2894–2902. doi:10.1109/TIE.2008.924207

Linares-Flores, J., Reger, J., & Sira-Ramírez, H. (2010). Load torque estimation and passivity-based control of a boost-converter/DC-motor combination. *IEEE Transactions on Control Systems Technology*, *18*(6), 1398–1405.

Loh, P.-C., Newman, M. J., Zmood, D. N., & Holmes, D. G. (2003). A comparative analysis of multiloop voltage regulation strategies for single and three-phase UPS systems. *IEEE Transactions on Power Electronics*, *18*(5), 1176–1185. doi:10.1109/TPEL.2003.816199

Mattavelli, P. (2001). Synchronous-frame harmonic control for high-performance AC power supplies. *IEEE Transactions on Industry Applications*, *37*(3), 864–872. doi:10.1109/28.924769

Mattavelli, P., Escobar, G., & Stankovic, A. M. (2001). Dissipativity-based adaptive and robust control of UPS. *IEEE Transactions on Industrial Electronics*, *48*(2), 334–343. doi:10.1109/41.915412

Ortega, R., Van Der Schaft, A., Maschke, B., & Escobar, G. (2002). Interconnection and damping assignment passivity-based control of port-controlled hamiltonian systems. *Automatica*, *38*(4), 585–596. doi:10.1016/S0005-1098(01)00278-3

Rymarski, Z. (2011). The discrete model of the power stage of the voltage source inverter for UPS. *International Journal of Electronics*, *98*(10), 1291–1304. doi:10.1080/00207217.2011.589736

Serra, F. M., De Angelo, C. H., & Forchetti, D. G. (2012a). Passivity-based control of a three-phase front end converter for stand alone wind generation system. In *Proceedings of the 10th IEEE/IAS International Conference on Industry Applications (INDUSCON)* (pp. 1–5). Fortaleza: IEEE.

Serra, F. M., De Angelo, C. H., & Forchetti, D. G. (2014). Interconnection and damping assignment control of a three-phase front end converter. *International Journal of Electrical Power & Energy Systems*, *60*, 317–324. doi:10.1016/j.ijepes.2014.03.033

Serra, F. M., De Angelo, C. H., Forchetti, D. G., & Garcia, G. O. (2012b). Non-linear control of a three-phase front end converter. In *Proceedings of the IEEE International Conference on Industrial Technology (ICIT)* (pp. 821–826). Athens: IEEE.

Singh, B., & Kasal, G. K. (2008). Solid state voltage and frequency controller for a stand alone wind power generating system. *IEEE Transactions on Power Electronics*, *23*(3), 1170–1177. doi:10.1109/TPEL.2008.921190

Tang, Y., Yu, H., & Zou, Z. (2008). Hamiltonian modeling and energy-shaping control of three-phase AC/DC voltage-source converters. In *Proceedings of the IEEE International Conference on Automation and Logistics (ICAL)* (pp. 591–595). Qingdao: IEEE.

Valderrama, G. E., Stankovic, A. M., & Mattavelli, P. (2003). Dissipativity-based adaptive and robust control of UPS in unbalanced operation. *IEEE Transactions on Power Electronics*, *18*(4), 1056–1062. doi:10.1109/TPEL.2003.813768

Wang, P., Wang, J., & Xu, Z. (2008). Passivity-based control of three phase voltage source PWM rectifiers based on PCHD model. In *Proceedings of the International Conference on Electrical Machines and Systems (ICEMS)* (pp. 1126–1130). Wuhan: IET.

Wang, Z., & Goldsmith, P. (2008). Modified energy-balancing-based control for the tracking problem. *IET Control Theory & Applications*, *2*(4), 310–322. doi:10.1049/iet-cta:20070124